ELSEVIER

Flash infrared annealing as a cost-effective and low environmental impact processing method for planar perovskite solar cells

Sandy Sánchez [1,2,†], Marta Vallés-Pelarda [3,†], Jaume-Adrià Alberola-Borràs [3,4], Rosario Vidal [4], José J. Jerónimo-Rendón [1], Michael Saliba [1,6,*], Pablo P. Boix [5,*], Iván Mora-Seró [3,*]

[1] Adolphe Merkle Institute University of Fribourg, Chemin des Verdiers 4, CH-1700 Fribourg, Switzerland
[2] Laboratory of Photomolecular Science (LSPM) École Polytechnique Fédérale de Lausanne (EPFL), 1015 Lausanne, Switzerland
[3] Institute of Advanced Materials (INAM), University Jaume I, Avenida de Vicent Sos Baynat, s/n, 12071 Castelló de la Plana, Spain
[4] Department of Mechanical Engineering and Construction, GID, Universitat Jaume I, Av. Sos Baynat s/n, 12071 Castelló de la Plana, Spain
[5] Instituto de Ciencia Molecular (ICMol), Universitat de València, Catedrático José Beltrán, 2, 46980 Paterna, Spain
[6] Institute of Materials Science, Technical University of Darmstadt, Alarich-Weiss-Strasse 2, D-64287 Darmstadt, Germany

For successful commercialization of perovskite solar cells, straightforward solutions in terms of environmental impact and economic feasibility are still required. Flash Infrared Annealing (FIRA) is a rapid method to fabricate perovskite solar cells with efficiencies >18% on simple, planar architecture, which allows a film synthesis in only 1.2 s, faster than the previous report based in a meso architecture and all of them without the usage of antisolvent. In this work, through a comparative study with the common lab-scale method, the so-called antisolvent (AS), the main photovoltaic parameters and working mechanisms obtained from impedance spectroscopy (IS) measurements show similar device features as for FIRA. However, from the life cycle assessment (LCA) comparison study, the FIRA method has only 8% of the environmental impact and 2% of the fabrication cost of the perovskite active layer with respect to the AS for the perovskite film synthesis. These results denote that FIRA is a low-impact, cost-effective fabrication approach that can be directly adapted to perovskite planar configuration that is compatible with industrial up-scaling.

Introduction

Perovskite solar cells (PSCs) have made impressive improvements in one decade with lab-scale efficiencies of 23.7% [1,2], comparable to other well-established solar cells materials. Consequently, the commercialization of PSCs is now a high-priority topic involving many research groups and companies worldwide [3–5]. This includes industrial up-scaling, which is a complex task, especially for such a recent technology that still faces challenges in terms of long-term stability, large-area deposition methods, reproducibility, low cost, and low environmental impact. Thus, a commercially successful fabrication technique should avoid treatments that are incompatible with large area fabrication processes. In addition, considerations on the environmental impact associated with the fabrication steps, as well as their energy consumption and materials employed, are key to achieve a viable industrial fabrication process [6–9].

In this work, we show that recently reported Flash Infrared Annealing (FIRA) is an easily scalable crystallization method for perovskite thin films without the need of a mesoporous, high-temperature scaffold. Through FIRA and using the planar architecture, we are able to reduce the synthesis time of the perovskite film until 1.2 s, which represents 29% less with respect to the

* Corresponding authors.
E-mail addresses: Saliba, M. (miliba@gmail.com, michael.saliba@opto.tu-darmstadt.de), Boix, P.P. (pablo.p.boix@uv.es), Mora-Seró, I. (sero@uji.es).
† Same contribution.

https://doi.org/10.1016/j.mattod.2019.04.021

synthesis time needed for the mesoporous TiO_2 electrode (1.7 s), as previously reported at the first time [10]. The lower synthesis time of the perovskite film is significant in terms of cost reduction in the manufacturing process. To date, the most efficient lab-scale PSCs fabrication procedure is the antisolvent (AS) method [11] where an antisolvent, typically chlorobenzene, is added suddenly to a perovskite precursor, typically dissolved in DMF or DMSO, inducing a supersaturation that triggers the perovskite nucleation process. Frequently, a relatively long annealing process of up to 1 h is required for the final crystallization. This method is challenging to up-scale [12]. In addition, AS is difficult to implement for large areas and requires an extra solvent and a long thermal annealing step affecting not just the cost but the environmental impact [13]. In contrast, FIRA uses a short IR flash in the range of seconds allowing for the fast nucleation and crystal growth of the perovskite film from the precursor solution. It is compatible with large area deposition techniques, such as slot dye or roll-to-roll processing. Consequently, FIRA is proposed as a feasible low cost and rapid thermal process for the production of perovskite thin films and corresponding devices [10,14].

Rapid thermal annealing is commonly used for semiconductors, e.g. silicon solar cells [8,15,16], to grow pure crystal phases without losing material quality, e.g. pure monocrystalline silicon. Large open-circuit voltage, V_{oc}, improvements were achieved by the removal of defects and dopant activation [15]. Silicon solar cells with efficiencies of 17.1 % were reported with rapid thermal processing in conjunction with surface passivation [17]. Similarly, the degradation of multicrystalline silicon solar cells can be reduced by 80% using a 10-s annealing treatment at 200 °C with a high-intensity irradiation of 44.8 kW m^{-1} [16]. In PSCs, rapid thermal process synthesis provides a cost-effective route to improve key structural properties in perovskite films [18–21].

For an exhaustive determination of environmental impacts, a life cycle assessment (LCA) methodology is commonly employed. In recent years, a significant number of LCA studies are performed in order to analyze PSCs for sustainable commercialization. Most of the studies are focused on the configuration of PSCs produced in the laboratories [13,22–26]. In general, these results criticize PSCs' lead content as a significant risk for the environment. However, the energy consumption emerges as the most demanding disadvantage during production and consequently is one of the most important thresholds to optimize the up-scaling process.

Here, we analyze the potential of FIRA related to industrially friendly process for PSCs. We compare the PSCs' performance of FIRA and AS, analyzing the cost of production and the environmental impact by LCA of both methods. We propose an extrapolation of the FIRA process to fabricate triple cation perovskite (methylammonium (MA)-formamidinium (FA)-Cs) films reporting for the first time a planar architecture. Planar PSCs are more attractive for industrial implementation than devices with mesoporous architecture as they present lower cost and environmental impacts [22]. Despite the multication perovskite increasing the cost compared to simpler, single-cation perovskites [13], the higher stability reported for multication perovskites can compensate the cost increase [27–32].

We show that FIRA results in compact perovskite films on FTO/TiO_2, simplifying the system complexity in view of potential industrial viability. These devices achieve a highly reproducible power conversion efficiency (PCE) of more than 18%, comparable to devices fabricated by AS. Optoelectrical characterization of films and devices by impedance spectroscopy unveils identical patters governing AS and FIRA solar cells, which suggests similar working principles. This was achieved with a modified FIRA setup that can quickly heat up the perovskite solution as compared to previous works with mesoporous architecture [10,14]. In the specific design developed for planar samples, the IR emitter can increase the temperature in the chamber up to 1000 °C in a few seconds and the cooling integrated system dissipates the heat quickly, thus enabling control on the crystallization kinetics of the thin film without thermal degradation. On the way of PSCs to commercialization, there are few examples of LCA studies, where the perovskite was deposited by processes suitable for industrial scale [33,34]. As far as we know, this is the first work reporting the LCA of high-temperature short-time annealing for PSCs' preparation, reporting a significant advantage with respect to commonly used lab techniques with an enormous potential for up-scaling.

Mixed cation perovskite thin-film analysis

Planar configuration has significant advantages from the up-scaling point of view in terms of low cost and low environmental impact when compared to architectures with a mesoporous TiO_2 layer [22]. Here, we show that the FIRA method can grow a planar smooth and compact perovskite layer. The optical microscope images shown in Fig. 1a unveil larger crystal domains for the planar compared to the mesoporous architecture. The rapid crystal growth across the substrate can avoid that the solution dewets on the planar substrate. Fig. 1b shows the transmittance spectra for the two samples depicted in Fig. 1a, where the planar

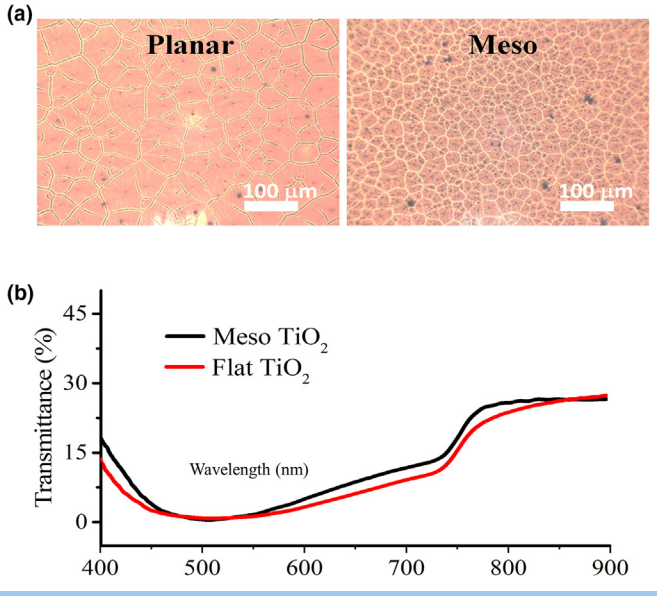

FIGURE 1

Perovskite films fabricated by FIRA on top of planar and meso architectures: (a) Optical microscope images taken in transmittance mode and, (b) the respective transmittance spectra.

configuration has lower transmittance than the meso case. This may be due to the greater effective optical absorption or the smaller light scattering of the perovskite film grown on a flat electrode. The characteristic FIRA grain domain has typically a large microstructure composed by highly oriented single grain-particles, as previously reported [10], see SEM pictures in Fig. 2a. This microstructure is formed through nucleation centers surrounded by ordered rings of single grains of 5 to 30 μm (as shown in Fig. S1 for planar electrodes). This thin film microstructure can play an important role in the final device performance [35,36].

To assess planar FIRA perovskite films, we compare them to state-of-the-art AS perovskite films. Fig. 2a and b shows SEM top-view images for FIRA and AS. Indeed, FIRA films have large domains of 40 μm. From Fig. 2b, we observe that the AS films have a typical grain size of 200 nm [37–39]. In addition, Fig. 2a shows the temperature profile for the FIRA-annealed film for the first 1.2 s, the temperature collected corresponds to the chamber (not directly to the film surface). Within this time, FIRA produces the crystallization of perovskite film, see Fig. 2c. The sample is kept in the chamber for 20 s to completely remove remaining solvents, reducing significantly the annealing time for AS that requires up to an hour, see Fig. 2b. Despite the morphological differences, FIRA and AS perovskite films present similar structural and optical characteristics in terms of XRD and PL characterization, see Fig. 2c. The diffraction pattern shows highly crystalline films with the tetragonal phase at room temperature which correspond to the mixed cations compounds with a large amount of FA (83%), which is stabilized by the addition of smaller cations, such as MABr (17%) and CsI (5%), as previously reported [27,40]. The PL emission spectra correspond to the band gap of the MAFACsPbIBr compound of about 1.6 eV and show in this case similar intensities and peak width [41–44]. Fig. 2d shows a cross sectional image of the manufactured devices comparing FIRA and AS. Both cases show the formation of pinhole-free and compact films.

PV performance and electronic characteristic of the devices

The regular architecture stack was used with FTO/TiO_2/MAFACsPbIBr/Spiro-OMetad/Au layers, as shown the SEM

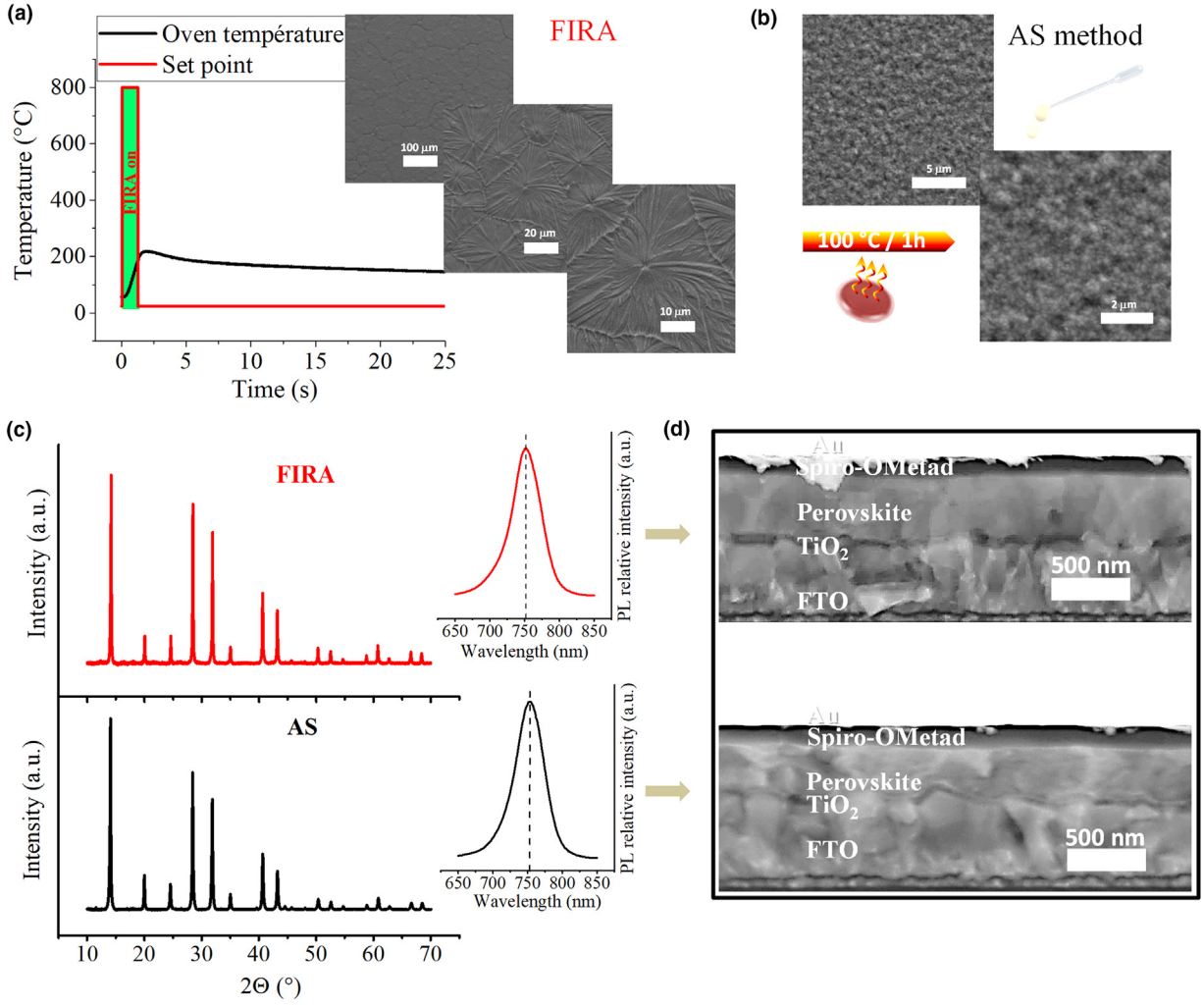

FIGURE 2

(a) Temperature profile of FIRA-annealed films with respective SEM top view. (b) SEM top-view image of the antisolvent-annealed films and a schematic inserted to illustrate the AS method. (c) XRD pattern (left) and photoluminescence spectra (right) of the FIRA and AS perovskite films. (d) Cross sectional images of the devices with FIRA and AS perovskite films.

cross-sectional image of Fig. 2d. The JV characteristic of the champion devices, Fig. 3a, shows similar PV parameters for both studied methods, achieving a PCE of more than 18%. The forward scan displays little hysteresis [45–47], and has PCEs > 17%. The high performance of these PSCs may also contribute to a decreased hysteresis [48]. In addition, samples prepared by FIRA and AS exhibit similar long-term stability, see Fig. S2. It is also worth to highlight that FIRA samples with higher area of 1.4 cm^2 preserve the photocurrent and the photovoltage, see Fig. S3. 14% of their efficiency is just reduced with respect to the performance of the low area devices, comparing high area devices in Fig. S3 with low area devices in Fig. 3. The main limitation of the efficiency high area devices, see Fig. S3, is due to the decrease in FF, which can be attributed to the increase in series resistance in the larger area device. Further device engineering will reduce this upscaling limitation. Fig. 3b compares FIRA and AS devices presenting statistics of the main PV parameters. Here the standard deviation demonstrates a good reproducibility for both methods. Note that the data points are more spaced for FIRA than AS, as the median values are a bit lower in the FIRA case. FIRA samples, however, present slightly higher FF dispersion as compared to samples fabricated by the antisolvent method. This dispersion cannot be attributed to series resistance differences, as similar values of ~10 Ω·cm^2, considering the experimental error, were obtained by impedance spectroscopy. We attribute the higher dispersion of FIRA samples to the synthesis in ambient conditions instead of the glovebox fabrication, as in the antisolvent samples. We point out that all the FIRA processing was carried out in a standard fume hood, with a relative humidity of ~30–40%. Thus, the film formation can be improved even further by standardizing the atmospheric conditions [46].

Further insights into the device working mechanisms can be obtained by means of impedance spectroscopy. The devices were measured under different light intensities at V_{oc} in order to evaluate charge recombination and charge storage behavior. The obtained Nyquist plot, with two distinguishable features at high and low frequency, were adjusted to a simplified equivalent circuit, (Fig. S4) as previously reported [49,50]. Although an in-depth model for PSCs is still under development, the results enable interesting observations regarding the operation mechanisms. On the first place, the high-frequency capacitance, which is associated to the perovskite geometric capacitance (C_g) [49], shows similar values for both FIRA and AS devices, see Fig. 4a. These values are in good agreement with previous reports, indicating a dielectric constant of $\varepsilon_r \sim 35$ regardless of the fabrication method. Similar low-frequency capacitance (C_{lf}) [51], with different interpretations in the literature but mostly pointing to an origin linked with ionic motion [52–55], suggests that both analyzed methods result in similar features in terms of ionic effect, see Fig. 4a. This observation is particularly interesting for the studied cases, as the grain size of the samples present clear differences. As a result of the similar charge distribution of the perovskites, the recombination behavior of the analyzed samples does not present significant disparities. In particular, an estimation of the charge recombination process can be extracted from

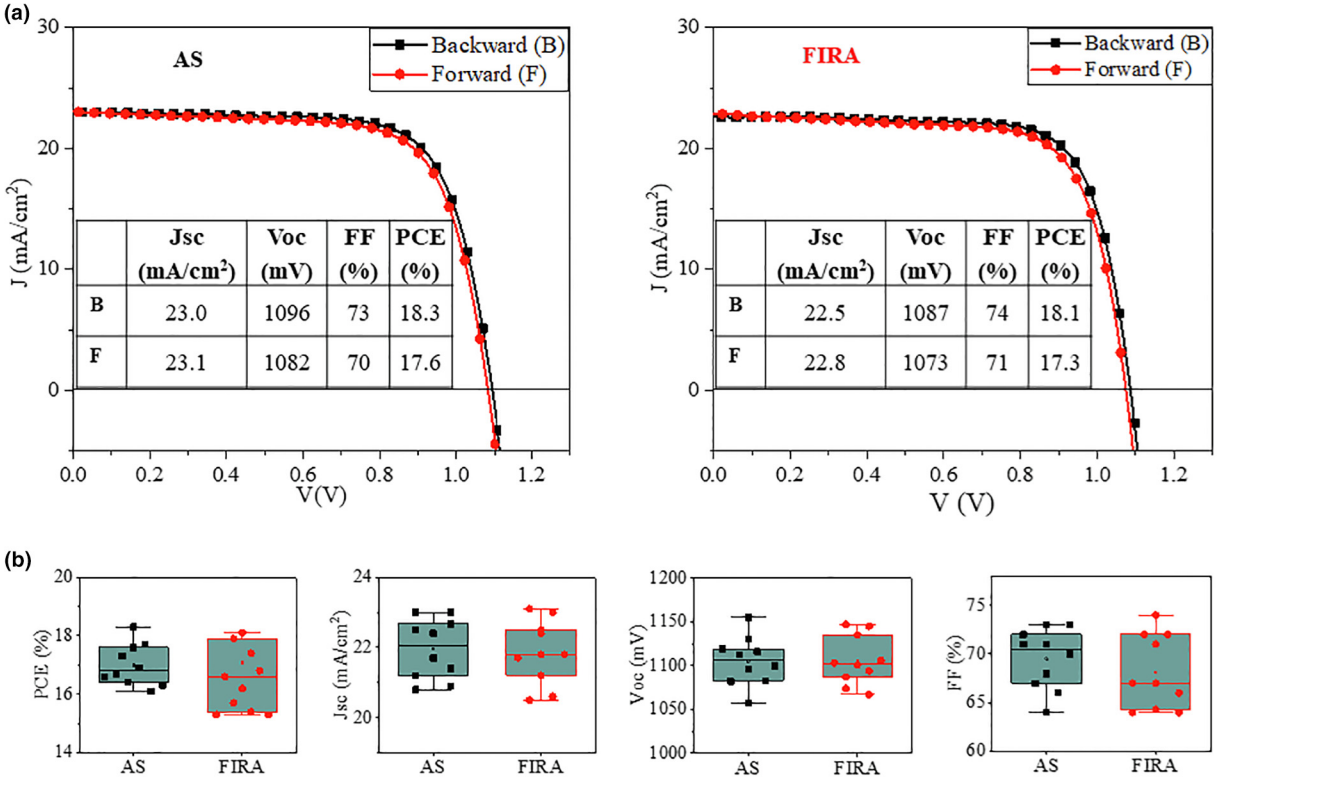

FIGURE 3

(a) Forward and backward JV scan of the champion devices made by FIRA and AS. The scan rate was 10 mV/s with an aperture area of 0.09 cm^2. (b) Statistic of the PV parameters for 10 devices made by FIRA and AS.

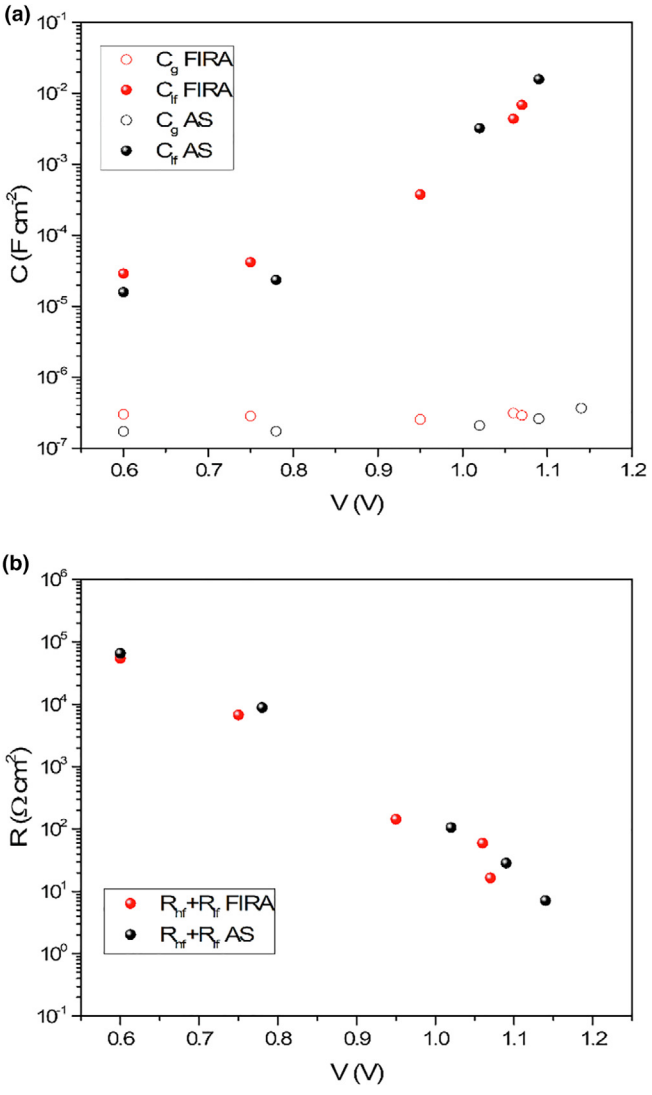

FIGURE 4

(a) Capacitive and (b) resistive parameters of FIRA- and AS-based perovskite solar cells measured under different light intensities at open circuit. The parameters are extracted from the fitting to the equivalent circuit discussed in the supporting information.

the series addition of the resistances in both high- and low-frequency features [50,56], displayed in Fig. 4b. The individual resistive components (R_{hf} for the high-frequency feature and R_{lf} for the low-frequency feature) are displayed in the Supporting Information, Fig. S5. These results highlight the fact that PSCs can present high performance with different apparent morphologies (i.e. high efficiency has been reported for PSCs based on evaporation with small grain size [57]). Consequently, morphology can have an effect on the final optoelectrical properties of the perovskite films, yet it is not the main factor determining the final photovoltaic performance of the device.

Life cycle assessment of the perovskite film synthesis methods

Finally, we have conducted an LCA to determine the potentiality of both processes for up-scalability. We have considered that both devices can preserve the same efficiencies on larger substrates, although this will be more difficult for AS samples [12]. Further considerations about the assumptions and methodology adopted for LCA can be found in the Materials and Methods section. Different impact categories have been analyzed for both kinds of samples, see Table 1 where abbreviations and units are also included. One of the most significant impact categories to measure the environmental performance of a solar energy collector device is the carbon footprint, as one of the main benefits from solar energy stemming is a reduced greenhouse effect. Photochemical oxidation and acidification are also selected to have a broad panoply.

Energy is a fundamental aspect of perovskite modules as it is their only valuable output. Knowing the necessary production energy is a good practice to calculate how viable their production is. The cumulative energy demand method V1.09 (CED) [58] obtains the total cradle-to-gate energy invested in the production of the perovskite module. Externalities need to be included as well for a holistic assessment. Thus, the potential toxicity of the production and emission of chlorobenzene and nitrogen was performed with USEtox V1.04 method [59], including the impact categories Human toxicity (cancer), Human toxicity (non-cancer), and Freshwater ecotoxicity, see Table 1. CML, CED, and USEtox methods are incorporated within the SimaPro® 8.0.3.14 software [60].

The environmental impacts and the cost are relativized with respect to the corresponding highest value for the two methods, FIRA and AS, using the same functional unit (1kWh). In this way, the results are independent of the solar cell lifetime. Life cycle inventories for 1 kWh are summarized in Table S1. AS method presents the highest environmental impacts in each of the categories considered and also the highest cost, for the system boundaries of Fig. 5, hence the value of 100 % is assigned in Fig. 6 and the values for the FIRA method are relative to the values of the AS method. Absolute values can be found in Table S2. Environmental impacts are disaggregated in the impacts produced by material acquisition, energy consumption during the processing and emissions, and transport. Costs are broken-down in materials and energy.

TABLE 1

List of impact categories, their abbreviations, units, and methodologies in which they are included.

Category	Abbreviation	Unit	Methodology
Climate change	GWP	kg CO_2 eq	CML baseline V3.02 [61]
Photochemical oxidation	POP	kg C_2H_4 eq	
Acidification	AP	kg SO_2 eq	
Cumulative energy demand	CED	MJ	Cumulative energy demand V1.09 [58]
Human toxicity, cancer effects	HTC	CTUh	Usetox V1.04 [59]
Human toxicity, non-cancer effects	HTNC	CTUh	
Freshwater ecotoxicity	ET	CTUe	

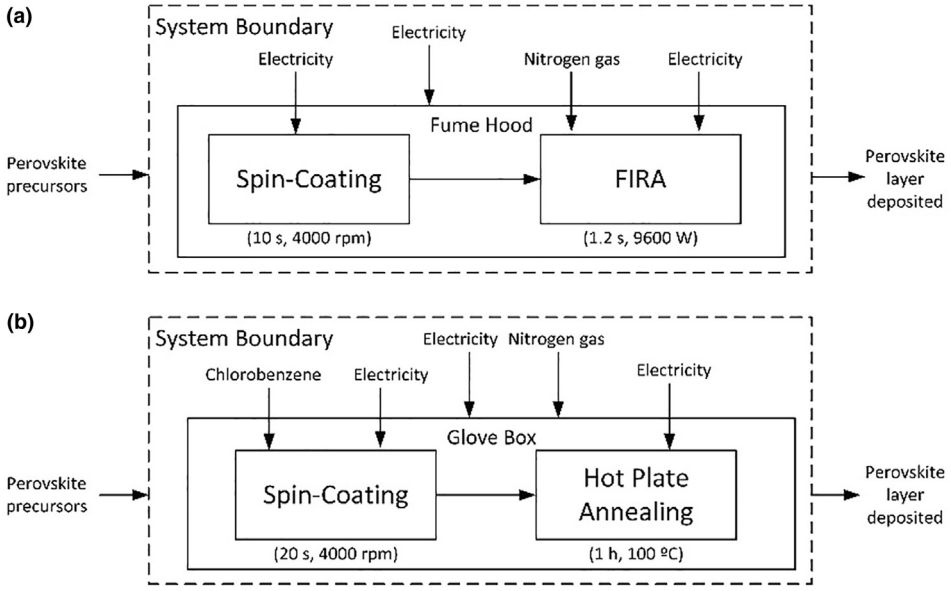

FIGURE 5

System boundaries for the perovskite layer deposition considering only the process that are different. (a) FIRA method. (b) Antisolvent method.

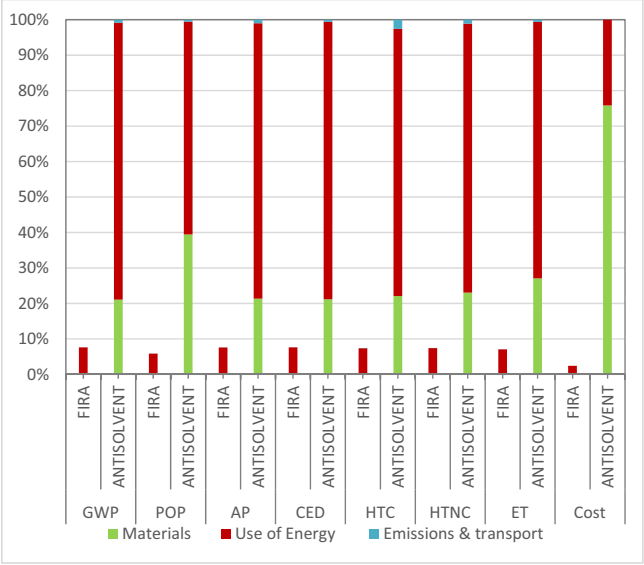

FIGURE 6

Relative costs and environmental impacts of the different process of the FIRA and antisolvent methods for perovskite layer deposition. Abbreviation of each impact category are explained in Table 1.

The environmental impacts of the AS method are mainly incurred by the energy consumption during the annealing, an often-disregarded factor. The substitution of the long AS annealing by the fast FIRA process implies significantly lower electricity consumption and also the elimination of chlorobenzene consumption that also have adverse contributions. The environmental impacts of the FIRA method are less than 8% compared to AS in all analyzed categories in Fig. 4. Annealing was also identified to have one of the highest environmental impacts on the LCA of a pre-industrial process based on a carbon stack architecture [34]. Moreover, the advantages of FIRA method in comparison with AS are not just in terms of impact but in terms of cost. The material prices have a significate influence (76%) in the cost of the antisolvent method. The reduction in nitrogen consumption, the absence of chlorobenzene, and the lower energy consumption in the FIRA method mean that the cost with this methodology is only 2% of the AS method.

Conclusions

We show that it is possible to fabricate planar perovskite solar cells using FIRA, which is compatible with up-scaling compared to the commonly used mesoporous configuration. Considering the PV performance and the impedance spectroscopy analysis, it can be concluded that the FIRA method can produce PSCs with similar efficiency than the commonly reported antisolvent methods. FIRA and AS present different morphology but similar optoelectronic performance in terms of PL and impedance spectroscopy, a fact that points to similar working principles in both devices. Finally, FIRA does not need an additional solvent, and the amount of energy is significantly reduced due to the much shorter annealing time of seconds instead of up to an hour. As a result, a systematic life cycle assessment has allowed us to determine that the cost and environmental impacts are decreased one order of magnitude comparing FIRA with AS. With the assumptions of the present work, the impacts caused by different processes reveal that FIRA exhibits only 8% of the impact of AS samples, for all the impact categories analyzed, while the cost is just 2%. This work highlights the potential of FIRA for up-scaling toward eventual commercialization.

Materials and methods

Device manufacturing

Photovoltaic devices were fabricated on FTO-coated glass (Pilkington NSG TEC™). The substrates were cleaned with Hellmanex soap, followed by 30-min sonication in a Hellmanex 2% water solution, 15-min sonication in IPA, and 5 min of oxygen plasma etching. Then, 30-nm-thick TiO_2 compact layers were deposited

onto the FTO by spray pyrolysis at 450 °C from a precursor solution of titanium diisopropoxide bis (acetylacetonate) in anhydrous ethanol and acetylacetone. After spraying, the FTO substrates were left at 450 °C for 5 min before cooling to room temperature. Then, a mesoporous TiO_2 layer was deposited by spin-coating for 10 s at 4000 rpm with a ramp of 2000 rpm s^{-1}, using a 30-nm particle size TiO_2 paste (Dyesol 30 NR-D) diluted in ethanol to achieve 150- to 200-nm-thick mesoporous layers. After spin-coating, the FTO substrates were dried at 100 °C for 10 min, and the films were annealed on a programmable hotplate (2000 W, Harry Gestigkeit GmbH) to crystallize TiO_2 at 450 °C for 30 min under dry air flow.

The hybrid perovskite precursor solutions were deposited from a precursor solution containing CH_5N_2I (1 M), PbI_2 (1.1 M), CH_3NH_3Br (0.2 M), and $PbBr_2$ (0.2 M) in anhydrous DMF: DMSO 2:1 (v:v). Note that this composition contains a lead excess as reported elsewhere [27]. Then CsI, dissolved as a 1.5 M stock solution in DMSO, was added to the mixed perovskite precursor to achieve the desired triple cation composition.

For antisolvent method the perovskite films were deposited as previously reported [47,62]. The perovskite solution was spin-coated in two steps at 1000 and 6000 rpm for 10 and 20 s, respectively. During the second step, 100 μL of chlorobenzene was poured onto the spinning substrate, 5 s before the end of the program. The substrates were then annealed at 100 °C for 1 h in a nitrogen-filled glovebox. After perovskite annealing, the substrates were cooled down within a few minutes.

The films made by FIRA method include the spin-coating of the perovskite solution in a single step at 4000 rpm for 10 s. The substrates were then IR irradiated for 1.2 s in the FIRA oven and were kept there for 20 additional seconds before removal and cooling within several minutes. FIRA processing was carried out in a standard fume hood. Immediately after cooling the perovskite films, a spiro-OMeTAD (Merck) solution (70×10^{-3} M in chlorobenzene) was deposited by spin-coating at 4000 rpm for 20 s. Spiro-OMeTAD was doped with Li-TFSI (Sigma–Aldrich), tris(2-(1H-pyrazol-1-yl)-4-*tert*-butylpyridine)-cobalt(III) tris(bis(trifluoromethylsulfonyl)imide) (FK209, Dynamo), and 4-*tert*-butylpyridine (TBP, Sigma–Aldrich). The molar ratios of the additives to spiro-OMeTAD were: 0.5, 0.03, and 3.3 for Li-TFSI, FK209, and TBP, respectively.

Material and device characterization

Scanning electron microscopy and energy dispersive x-ray spectroscopy were carried out on a Tescan MIRA 3 LMH with a field emission source operated at an acceleration voltage of 10 kV using an octane-pro EDS detector. Powder X-ray diffraction was performed in transmission geometry with Cu target ($\lambda = 1.5401$ Å) using an STOE STADI P diffractometer. Optical transmission measurements were performed using a Zeiss AxioScope A1 Pol, a Zeiss EC Epiplan-Apochromat 20× objective, and a xenon light source (Ocean Optics HPX-2000). For spectroscopic measurements, an optical fiber (QP230-2-XSR, 230-μm core) collected the light reflected from the sample. The spectra were recorded by a spectrometer (Ocean Optics Maya2000 Pro), and a standard white diffuser was used as reference. Photoluminescence spectra were obtained with Fluorolog 322 (Horiba Jobin Ybon Ltd) with the range of wavelength from 620 nm to 850 nm by exciting at 460 nm. The samples were mounted at 60° and the emission recorded at 90° from the incident beam path.

The temperature in the FIRA chamber was measured using a K-type thermocouple and the surface temperature of the FTO was measured by a wire J-type thermocouple, both connected to an Analog Devices *AD595* amplifier interfaced with Labview software. Impedance Spectroscopy measurements were performed using a PGSTAT-30 Autolab potentiostat and a Xe lamp [63]. The light intensity was controlled using different neutral density filters.

Life cycle assessment

A comparative life cycle assessment (LCA) is performed focused on the deposition layer of perovskite for both antisolvent and FIRA methods. 1 kWh of energy is assumed to be produced by each one of these two methods. This kWh of electricity was simulated to be produced assuming the current power conversion efficiency values and the fill factors of each device [10], the Direct Normal Irradiance in Fribourg (1275 $kW{\cdot}m^{-2}{\cdot}year^{-1}$) [64] and considering 400 h of work [65]. The size of the substrate is 5 × 5 cm.

The system boundaries for the comparative LCA are shown in Fig. 5, where just the processes that are different AS are considered. Therefore, the common processes for the FIRA and the AS methods are not considered. Energy and nitrogen consumption in the FIRA process are experimentally measured. Energy consumption for spin-coating and hot plate annealing were obtained in a previous study [13]. Nitrogen gas and electricity consumption in the glovebox are obtained from its technical specifications, considering the maximum nitrogen leak rate (PureLab HE 2 GB). Electricity consumption in the fume hood is for a standard exhaust blower (1/3 hp). The same amount of perovskite precursors for the two methods is estimated and they are not included in the LCA. The detailed inventory is included in the Supplementary material. Materials and electricity are modeled with the Ecoinvent 3.3 database using processes for Europe.

Costs for the two methods considered are obtained from their life cycle inventories for the system boundaries of Fig. 5. Electricity price of 0.112 €/kWh is the EU-28 weighted average price using national data for the quantity of consumption by non-household consumers [66]. The material prices are obtained from the suppliers and include transport costs.

Data availability

Data will be available on request.

Acknowledgments

S.S., J.J.J., and M.S. acknowledge the Adolphe Merkle and the Swiss National Science Foundation (Program NRP70 No. 153990). M.V.-P. and I.M.-S. acknowledge the support of the European Research Council (ERC) via Consolidator Grant (724424 - No-LIMIT). M.V.-P. also acknowledges Universitat Jaume I for the support through FPI Fellowship Program (PREDOC/2017/40). P.P.B. acknowledges the financial support from Generalitat Valenciana (SEJI2017/2017/012).

Appendix A. Supplementary data

Supplementary data to this article can be found online at https://doi.org/10.1016/j.mattod.2019.04.021.

References

[1] D. Yang, R. Yang, K. Wang, C. Wu, X. Zhu, J. Feng, X. Ren, G. Fang, S. Priya, S. Liu, Nat. Commun. 9 (2018) 3239.

[2] N.J. Jeon, H. Na, E.H. Jung, T.-Y. Yang, Y.G. Lee, G. Kim, H.-W. Shin, S. Il Seok, J. Lee, J. Seo, Nat. Energy 3 (2018) 682–689.

[3] W. Chen, Y. Wu, Y. Yue, J. Liu, W. Zhang, X. Yang, H. Chen, E. Bi, I. Ashraful, M. Grätzel, L. Han, Science 350 (2015) 944–948.

[4] K. Hwang, Y.-S. Jung, Y.-J. Heo, F.H. Scholes, S.E. Watkins, J. Subbiah, D.J. Jones, D.-Y. Kim, D. Vak, Adv. Mater. 27 (2015) 1241–1247.

[5] Y.-S. Jung, K. Hwang, Y.-J. Heo, J.-E. Kim, D. Vak, D.-Y. Kim, Adv. Opt. Mater. 6 (2018) 1701182.

[6] A.G. Aberle, Thin Solid Films 517 (2009) 4706–4710.

[7] M. Hörteis, S.W. Glunz, Prog. Photovoltaics Res. Appl. 16 (2008) 555–560.

[8] N. Kazuo, A. Michio, W. Naozo, Jpn. J. Appl. Phys. 19 (1980) L563.

[9] A. Rohatgi, Z. Chen, P. Doshi, T. Pham, D. Ruby, Appl. Phys. Lett. 65 (1994) 2087–2089.

[10] S. Sanchez, X. Hua, N. Phung, U. Steiner, A. Abate, Adv. Energy Mater. 8 (2018). 1702915-n/a.

[11] N.J. Jeon, J.H. Noh, Y.C. Kim, W.S. Yang, S. Ryu, S.I. Seok, Nat. Mater. 13 (2014) 897–903.

[12] Y. Jiang, M.R. Leyden, L. Qiu, S. Wang, L.K. Ono, Z. Wu, E.J. Juarez-Perez, Y. Qi, Adv. Funct. Mater. 28 (2018) 1703835.

[13] J.-A. Alberola-Borràs, R. Vidal, I. Mora-Seró, Sustainable Energy Fuels 2 (2018) 1600–1609.

[14] S. Sanchez, N. Christoph, B. Grobety, N. Phung, U. Steiner, M. Saliba, A. Abate, Adv. Energy Mater. 8 (2018) 1802060.

[15] M.L. Terry, A. Straub, D. Inns, D. Song, A.G. Aberle, Appl. Phys. Lett. 86 (2005) 172108.

[16] D.N.R. Payne, C.E. Chan, B.J. Hallam, B. Hoex, M.D. Abbott, S.R. Wenham, D. M. Bagnall, Sol. Energy Mater. Sol. Cells 158, Part 1 (2016) 102–106.

[17] P. Doshi, A. Rohatgi, M. Ropp, Z. Chen, D. Ruby and D. L. Meier, 1994.

[18] J. Xu, Z. Hu, X. Jia, L. Huang, X. Huang, L. Wang, P. Wang, H. Zhang, J. Zhang, J. Zhang, Y. Zhu, Org. Electron. 34 (2016) 84–90.

[19] J. Troughton, C. Charbonneau, M.J. Carnie, M.L. Davies, D.A. Worsley, T.M. Watson, J. Mater. Chem. A 3 (2015) 9123–9127.

[20] J. Troughton, M.J. Carnie, M.L. Davies, C. Charbonneau, E.H. Jewell, D.A. Worsley, T.M. Watson, J. Mater. Chem. A 4 (2016) 3471–3476.

[21] J. Ye, H. Zheng, L. Zhu, X. Zhang, L. Jiang, W. Chen, G. Liu, X. Pan, S. Dai, Sol. Energy Mater. Sol. Cells 160 (2017) 60–66.

[22] J.-A. Alberola-Borràs, R. Vidal, E.J. Juárez-Pérez, E. Mas-Marzá, A. Guerrero, I. Mora-Seró, Sol. Energy Mater. Sol. Cells (2017), https://doi.org/10.1016/j.solmat.2017.11.008.

[23] L. Serrano-Lujan, N. Espinosa, T.T. Larsen-Olsen, J. Abad, A. Urbina, F.C. Krebs, Adv. Energy Mater. 5 (2015). 1501119-n/a.

[24] N. Espinosa, L. Serrano-Luján, A. Urbina, F.C. Krebs, Sol. Energy Mater. Sol. Cells 137 (2015) 303–310.

[25] J. Gong, S.B. Darling, F. You, Energy Environ. Sci. 8 (2015) 1953–1968.

[26] J. Zhang, X. Gao, Y. Deng, B. Li, C. Yuan, ChemSusChem 8 (2015) 3882–3891.

[27] M. Saliba, T. Matsui, J.-Y. Seo, K. Domanski, J.-P. Correa-Baena, M.K. Nazeeruddin, S.M. Zakeeruddin, W. Tress, A. Abate, A. Hagfeldt, M. Gratzel, Energy Environ. Sci. 9 (2016) 1989–1997.

[28] S. Kim, S. Bae, S.-W. Lee, K. Cho, K.D. Lee, H. Kim, S. Park, G. Kwon, S.-W. Ahn, H.-M. Lee, Y. Kang, H.-S. Lee, D. Kim, Sci. Rep. 7 (2017) 1200.

[29] C. Quarti, E. Mosconi, J.M. Ball, V. D'Innocenzo, C. Tao, S. Pathak, H.J. Snaith, A. Petrozza, F. De Angelis, Energy Environ. Sci. 9 (2016) 155–163.

[30] G. Abdelmageed, C. Mackeen, K. Hellier, L. Jewell, L. Seymour, M. Tingwald, F. Bridges, J.Z. Zhang, S. Carter, Sol. Energy Mater. Sol. Cells 174 (2018) 566–571.

[31] T.A. Berhe, W.-N. Su, C.-H. Chen, C.-J. Pan, J.-H. Cheng, H.-M. Chen, M.-C. Tsai, L.-Y. Chen, A.A. Dubale, B.-J. Hwang, Energy Environ. Sci. 9 (2016) 323–356.

[32] A. Calloni, A. Abate, G. Bussetti, G. Berti, R. Yivlialin, F. Ciccacci, L. Duò, J. Phys. Chem. C 119 (2015) 21329–21335.

[33] I. Celik, Z. Song, A.J. Cimaroli, Y. Yan, M.J. Heben, D. Apul, Sol. Energy Mater. Sol. Cells 156 (2016) 157–169.

[34] J.-A. Alberola-Borràs, J.A. Baker, F. De Rossi, R. Vidal, D. Beynon, K.E.A. Hooper, T.M. Watson, I. Mora-Seró, iScience 9 (2018) 542–551.

[35] W.A. Dunlap-Shohl, Y. Zhou, N.P. Padture, D.B. Mitzi, Chem. Rev. 119 (2019) 3193–3295.

[36] Y. Zhou, O.S. Game, S. Pang, N.P. Padture, J. Phys. Chem. Lett. 6 (2015) 4827–4839.

[37] G. Niu, W. Li, J. Li, X. Liang, L. Wang, RSC Adv. 7 (2017) 17473–17479.

[38] A.R. Pascoe, Q. Gu, M.U. Rothmann, W. Li, Y. Zhang, A.D. Scully, X. Lin, L. Spiccia, U. Bach, Y.-B. Cheng, Sci. China Mater. 60 (2017) 617–628.

[39] X. Zhou, Y. Zhang, W. Kong, M. Hu, L. Zhang, C. Liu, X. Li, C. Pan, G. Yu, C. Cheng, B. Xu, J. Mater. Chem. A 6 (2018) 3012–3021.

[40] D.P. McMeekin, G. Sadoughi, W. Rehman, G.E. Eperon, M. Saliba, M.T. Hörantner, A. Haghighirad, N. Sakai, L. Korte, B. Rech, M.B. Johnston, L.M. Herz, H.J. Snaith, Science 351 (2016) 151–155.

[41] N.J. Jeon, J.H. Noh, W.S. Yang, Y.C. Kim, S. Ryu, J. Seo, S.I. Seok, Nature 517 (2015) 476–480.

[42] D. Bi, W. Tress, M.I. Dar, P. Gao, J. Luo, C. Renevier, K. Schenk, A. Abate, F. Giordano, J.-P. Correa Baena, J.-D. Decoppet, S.M. Zakeeruddin, M.K. Nazeeruddin, M. Grätzel, A. Hagfeldt, Sci. Adv. (2016) 2.

[43] S. Draguta, O. Sharia, S.J. Yoon, M.C. Brennan, Y.V. Morozov, J.S. Manser, P.V. Kamat, W.F. Schneider, M. Kuno, Nat. Commun. 8 (2017) 200.

[44] N. Pellet, P. Gao, G. Gregori, T.Y. Yang, M.K. Nazeeruddin, J. Maier, M. Grätzel, Angew. Chem. Int. Ed. 53 (2014) 3151–3157.

[45] E.L. Unger, E.T. Hoke, C.D. Bailie, W.H. Nguyen, A.R. Bowring, T. Heumüller, M. G. Christoforo, M.D. McGehee, Energy Environ. Sci. 7 (2014) 3690–3698.

[46] B. Chen, M. Yang, S. Priya, K. Zhu, J. Chem. Phys. Lett. 7 (2016) 905–917.

[47] H.J. Snaith, A. Abate, J.M. Ball, G.E. Eperon, T. Leijtens, N.K. Noel, S.D. Stranks, J.T.-W. Wang, K. Wojciechowski, W. Zhang, J. Phys. Chem. Lett. 5 (2014) 1511–1515.

[48] M.T. Neukom, S. Züfle, E. Knapp, M. Makha, R. Hany, B. Ruhstaller, Sol. Energy Mater. Sol. Cells 169 (2017) 159–166.

[49] A. Guerrero, G. Garcia-Belmonte, I. Mora-Sero, J. Bisquert, Y.S. Kang, T.J. Jacobsson, J.-P. Correa-Baena, A. Hagfeldt, J. Phys. Chem. C 120 (2016) 8023–8032.

[50] I. Zarazua, G. Han, P.P. Boix, S. Mhaisalkar, F. Fabregat-Santiago, I. Mora-Seró, J. Bisquert, G. Garcia-Belmonte, J. Phys. Chem. Lett. 7 (2016) 5105–5113.

[51] E.J. Juarez-Perez, R.S. Sanchez, L. Badia, G. Garcia-Belmonte, Y.S. Kang, I. Mora-Sero, J. Bisquert, J. Phys. Chem. Lett. 5 (2014) 2390–2394.

[52] D.A. Jacobs, H. Shen, F. Pfeffer, J. Peng, T.P. White, F.J. Beck, K.R. Catchpole, J. Appl. Phys. 124 (2018) 225702.

[53] D. Moia, I. Gelmetti, P. Calado, W. Fisher, M. Stringer, O. Game, Y. Hu, P. Docampo, D. Lidzey, E. Palomares, J. Nelson and P. R. F. Barnes, arXiv, 2018, 1805.06446v06442.

[54] I. Zarazua, J. Bisquert, G. Garcia-Belmonte, J. Phys. Chem. Lett. 7 (2016) 525–528.

[55] M. Bag, L.A. Renna, R.Y. Adhikari, S. Karak, F. Liu, P.M. Lahti, T.P. Russell, M.T. Tuominen, D. Venkataraman, J. Am. Chem. Soc. 137 (2015) 13130–13137.

[56] Z. Zolfaghari, E. Hassanabadi, D. Pitarch-Tena, S.J. Yoon, Z. Shariatinia, J. van de Lagemaat, J.M. Luther, I. Mora-Seró, ACS Energy Lett. 4 (2019) 251–258.

[57] D. Pérez-del-Rey, P.P. Boix, M. Sessolo, A. Hadipour, H.J. Bolink, J. Phys. Chem. Lett. 9 (2018) 1041–1046.

[58] R. Frischknecht, N. Jungbluth, H.-J. Althaus, G. Doka, R. Dones, T. Heck, S. Hellweg, R. Hischier, T. Nemecek, G. Rebitzer, M. Spielmann, Int. J. Life Cycle Assess. 10 (2005) 3–9.

[59] R.K. Rosenbaum, T.M. Bachmann, L.S. Gold, M.A.J. Huijbregts, O. Jolliet, R. Juraske, A. Koehler, H.F. Larsen, M. MacLeod, M. Margni, T.E. McKone, J. Payet, M. Schuhmacher, D. van de Meent, M.Z. Hauschild, Int. J. Life Cycle Assess. 13 (2008) 532.

[60] Pré Sustainability, 2016. SimaPro.

[61] O. Jolliet, M. Margni, R. Charles, S. Humbert, J. Payet, G. Rebitzer, R. Rosenbaum, Int. J. Life Cycle Assess. 8 (2003) 324.

[62] J.M. Ball, M.M. Lee, A. Hey, H.J. Snaith, Energy Environ. Sci. 6 (2013) 1739–1743.

[63] D. Pitarch-Tena, T.T. Ngo, M. Vallés-Pelarda, T. Pauporté, I. Mora-Seró, ACS Energy Lett. 3 (2018) 1044–1048.

[64] The World Bank Group Global Solar Atlas Available at: https://globalsolaratlas.info/ 2016 Accessed November 21, 2018.

[65] B. McKenna, J.R. Troughton, T.M. Watson, R.C. Evans, RSC Adv. 7 (2017) 32942–32951.

[66] Eurostat (2018). Electricity price statistics - Statistics Explained. Eur. Comm. Available at: https://ec.europa.eu/eurostat/statistics-explained/index.php/Electricity_price_statistics#Electricity_prices_for_non-household_consumers [Accessed November 23, 2018].